DALTON
FULL PAPER

An investigation of C–S bond activation in transition metal crown thioether complexes using extended Hückel theory and electrospray mass spectrometry

Gregory E. D. Mullen,[a] Thomas F. Fässler,[b] Michael J. Went,[a] Kevin Howland,[a] Bridget Stein[c] and Philip J. Blower*[a]

[a] *Departments of Physical Sciences and Biosciences, University of Kent, Canterbury, UK CT2 7NJ*
[b] *Laboratorium für Anorganische Chemie, ETH Zürich, Switzerland*
[c] *EPSRC National Mass Spectrometry Service Centre, University of Wales, Swansea, UK SA2 8PP*

Received 23rd July 1999, Accepted 23rd September 1999

Complexes of Re and Tc with 1,4,7-trithiacyclononane (9S3) differ from their later transition metal analogues in that their d^6 form ($[M(9S3)_2]^+$) undergoes instantaneous C–S bond cleavage yielding ethene and $[M(9S3)L]^+$ (L = $SCH_2CH_2SCH_2CH_2S$), a stable metal(III) thiolate complex, cleanly in aqueous solution. This contrast is interpreted as signifying increased π-back donation by Re and Tc, compared to later metals, into ligand C–S σ* orbitals. In order to validate this hypothesis within an established theoretical framework, and to compare the predicted relative C–S bond lability with relative experimental lability in a series of d^6 analogues, extended Hückel theory (EHT) was used to investigate the bonding (M = Mo, Tc, Ru, Rh or Pd) while electrospray mass spectrometry (ES-MS) was used to compare ethene loss, in a series of analogous complexes (M = Tc, Re, Ru or Os). The C–S overlap populations were smaller for $M = Tc^{II}$ and Tc^{I} than for later metal(II) analogues, and were smaller for Tc^{I} than for Tc^{II}. Fragment molecular orbitals corresponding to C–S σ* were more highly populated for $M = Tc^{II}$ and Tc^{I} than for later analogues, and also more highly populated for Tc^{I} than for Tc^{II}. ES-MS showed that ethene loss from Tc/Re^{I} and Tc/Re^{II} complexes occurred at much lower energies than from the Ru/Os^{II} analogues. EHT supports the hypothesis that C–S activation is caused by π-back donation into C–S σ* orbitals, and correctly predicts that ethene loss occurs more readily from rhenium and technetium d^5 and especially d^6 complexes than from later transition metal analogues.

Introduction

Recently we reported an unusual C–S bond cleavage reaction from the complexes $[M(9S3)_2]^{2+}$ (M = Tc or Re; 9S3 = 1,4,7-trithiacyclononane) in which ethene is evolved quantitatively under mild conditions following one-electron reduction of the complexes with a variety of reducing agents to give $[M(9S3)L]^+$ (L = $SCH_2CH_2SCH_2CH_2S$), according to eqn. (1).[1]

$$[Re(9S3)_2]^{2+} + e \longrightarrow \text{“}[Re(9S3)_2]^{+}\text{”} \longrightarrow [Re(9S3)(SCH_2CH_2SCH_2CH_2S)]^+ + C_2H_4 \quad (1)$$

Related reductively induced alkene elimination reactions have previously been observed to be induced by electrochemical electron transfer to $[ReS_2(1,2\text{-dithiolate})]^-$ (to yield $[ReS_4]^-$) and to complexes of Mo, Fe and Ni of thioether–thiol chelating agents $HSC_6H_4S(CH_2CH_2S)_nC_6H_4SH$ ($n = 1$ or 2) to yield benzene-1,2-dithiolate complexes.[2] These examples share the property that the alkene loss is believed to occur from an intermediate in which the metal is in an oxidation state that is unusually low for its particular ligand environment. Ethene elimination, though not electron-transfer-induced, has also been observed from other complexes containing SCH_2CH_2S linkages including ethanedithiolate complexes of molybdenum and rhenium[3] and there are numerous examples of high-temperature breakdown of 9S3 and related thioethers at polynuclear metal centres.[4] Cleavage of a single C–S bond as a consequence of base-induced deprotonation of the 9S3 ligand has also been identified, although this is probably mechanistically unrelated to the reaction described in this paper.[5]

Behaviour analogous to that represented by eqn. (1) was not observed for 9S3 complexes of metals to the right of Tc and Re in the Periodic Table, suggesting that the activation of the C–S bond is dependent on the population and energy of the metal d orbitals. These observations can be rationalised in terms of π-back bonding by donation of electron density from the filled metal t_{2g} orbitals of the idealised octahedral metal ion, into ligand acceptor orbitals with C–S antibonding (σ*) character. This is drawn from the analogy with metal complexes containing tertiary phosphine ligands. The ability of phosphine ligands to act as π acceptors is well established, and recently it has become accepted that the primary contributor to this capacity is the presence of low-lying C–P σ* orbitals (rather than phosphorus d orbitals) of appropriate symmetry to interact with filled metal d orbitals.[6] X-Ray crystallographic data on metal phosphine complexes have been collected in support of this mechanism.[7] There is spectroscopic evidence that thioethers too have π-acceptor capacity.[8] That an analogous mechanism to account for the π-acceptor capacity of thioethers (*i.e.* involving C–S σ* orbitals as acceptors) occurs in thioether complexes has been suggested previously.[9]

The extensive series of structurally characterised bis-9S3 complexes now available (M = Fe to Zn, Tc to Cd and Re to Hg)[10] provides an opportunity to investigate the role of the thioether group as a π acceptor, by comparison within a series of structurally similar complexes of different metals in different oxidation states. The strength of the M–S backbonding interaction, and hence the degree of weakening of the C–S bonds, would be expected to increase as the metal d-orbital energy increases, *i.e.* on moving to the left in the transition metal

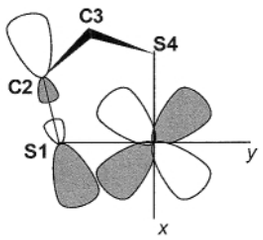

Fig. 1 Diagram to show notional overlap between "in-plane" C–S σ* and metal t_{2g} orbitals. Atoms S1, C2, S4 and the metal atom are coplanar, but C3 lies out of this plane, reducing the effective overlap of the C3–S4 σ* orbital with the metal d_{xy} orbital.

periods. In this interpretation, for rhenium and technetium the C–S activation is sufficient to induce immediate ethene formation upon reduction of the d^5 $[M(9S3)_2]^{2+}$ complexes to their d^6 counterparts. On the other hand, for the metals to the right of technetium and rhenium the activation is not sufficient to induce facile C–S bond cleavage under mild conditions.

The hypothesis that this C–S bond cleavage represents one extreme of a periodic trend is supported qualitatively by an analysis of the C–S bond lengths in an extensive series of analogous $[M(9S3)_2]^{2+}$ complexes, which shows C–S bond lengths increasing as the periodic group number of the metal decreases.[1] Moreover, this analysis demonstrated that C–S bond lengthening was more significant in C–S bonds lying in the plane of the metal t_{2g} orbitals (Fig. 1 and 2) than for those slightly out of the plane. This would be expected on the basis that overlap between metal t_{2g} and C–S σ* orbitals is better if the C–S bonds and the t_{2g} orbitals are coplanar than if they are not.[1]

In this paper we present both theoretical (within the accepted framework of extended Hückel theory, EHT) and experimental (from chemical and mass spectroscopic evidence) support for this model. Despite its well known limitations, the EHT approach was chosen because it can give good results in comparing trends in series of related compounds and geometries, while being economical with computing resources. We wished to compare the periodic trends in C–S bond reactivity predicted by the theory, with an experimental determination of the ease of ethene loss. Since under solution conditions we have been unable to observe ethene loss in any complexes except those of rhenium and technetium,[1] we sought an experimental setting that would provide the necessary activation energy to induce ethene loss in the less reactive complexes, enabling them to be quantitatively compared with rhenium and technetium. Here we describe results suggesting that electrospray mass spectroscopy (ES-MS) provides this. The trends observed experimentally in this system are compared with the predictions from EHT. The results have implications for the understanding of metal–sulfur bonding which may be significant in wider contexts such as hydrodesulfurisation catalysis and enzymatic reactions in which C–S bond cleavage at a metal centre is a part of the mechanism.[11]

Results and discussion

Extended Hückel calculations

In this investigation molecular orbital parameters relevant to the activation of C–S bonds by the mechanism suggested above were calculated and compared, as follows. First, trends in charge-iterated d-orbital energies for $[M(9S3)_2]^{2+}$ and $[M(9S3)_2]^{+}$ complexes were investigated (including M = Cr, Mn or Mo, complexes which have hitherto not been synthesized). Secondly, molecular orbitals were calculated and the Mulliken overlap population between carbon and sulfur atoms in the different complexes and in the "free" ligand were compared, to suggest trends in overall relative C–S bond strength changes due to interaction with the metals. Thirdly, the specific metal–ligand orbital interactions affecting the net C–S bonding were identified using the Fragment Molecular Orbital (FMO) approach in which ligand molecular orbitals are allowed to overlap with metal atomic orbitals. Fourthly, the FMOPOP populations of ligand orbitals that have C–S antibonding (σ*) character were calculated and compared for different metals and different oxidation states.

Table 1 Idealised bond lengths (Å) and angles (°) for the $[M(9S3)_2]^{n+}$ model complex

M–S	2.300	S–M–S	90
C–S	1.830	M–S–C	105.5
C–C	1.500	S–C–C	111.5
C–H	1.100	S–C–H	109.5
		C–C–S–M	±24

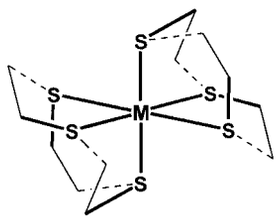

Fig. 2 Diagram to show idealised structure of $[M(9S3)_2]^{n+}$ complexes. The M–S and in-plane C–S bonds are shown as bold lines; out-of-plane C–S bonds are shown as broken lines.

As a basis for the relevant calculations, an idealised model structure for the $[M(9S3)_2]^{n+}$ complexes (Fig. 2), with fixed M–S, C–S, C–C and C–H bond distances the same regardless of the identity and oxidation state of M, was constructed. The parameters used are given in Table 1. This universal model was used in preference to the crystallographically determined geometries of individual complexes, so that changes in orbital populations and energies (resulting from changes in metal and oxidation state) could be compared without interference from the real geometric consequences of these changes. Precedent for this approach was set by Hoffmann *et al.*[12] in identifying the Mulliken population difference between equatorial and axial P–H bonds in PH_5. We have performed some of the calculations also using the crystallographically determined geometries. These results are not reported here in detail: the trends observed were (predictably) found to be somewhat exaggerated compared to those found in the fixed-geometry approach.

Charge iterated d-orbital energies. The intuitive model, given above, of the comparative bonding in the complexes as a function of period group number depends upon a progressive increase in d-orbital energies on moving from right to left in the transition series. Since the character of the calculated molecular orbitals is expected to be strongly dependent on the metal and sulfur valence orbital energies, the MEHMACC self-consistent charge iteration routine was used to obtain optimum Hückel parameters H_{ii} for the metal (Table 2) and sulfur (Table 3) valence orbitals in the idealised complexes $[M(9S3)_2]^{2+}$ and $[M(9S3)_2]^{+}$ (M = Cr to Cu and Mo to Pd). The optimised H_{dd} parameters correspond to the energies of the metal d orbitals, and the trends in their values for all the $[M(9S3)_2]^{2+}$ and $[M(9S3)_2]^{+}$ complexes, together with the default (non-charge iterated) values, are shown in Fig. 3. Three salient points emerge. First, the H_{dd} charge iterated values are significantly higher than the default values for all M^+ complexes and all M^{2+} complexes except for Cu^{2+} and Pd^{2+}. This suggests that, without charge iteration, metal to ligand π-backbonding effects are likely to be underestimated. Secondly, the charge iterated H_{dd} values decrease smoothly and progressively on moving to the right in the Periodic Table (except for Mn for which no bis(9S3) complexes are known), as required by the intuitive model. This suggests that, other factors being equal, π-back-

Table 2 Details of metal charge iterations

Orbital	H_{ii}/eV					Exponents[a]	
	Default	+1	+2	+3	+4	ζ_1	ζ_2
Mo 4d	−10.5	−6.58	−8.59	—	—	4.54 (0.5899)	1.90 (0.5899)
5p	−5.24	−2.83	−4.08	—	—	1.90	
5s	−8.34	−5.52	−6.98	—	—	1.96	
Tc 4d	−12.82	−7.04	−9.18	—	—	4.90 (0.5715)	2.09 (0.6012)
5p	−5.40	−2.51	−3.83	—	—	1.90	
5s	−10.07	−5.30	−6.85	—	—	1.90	
Ru 4d	−14.90	−8.05	−9.77	−11.65	—	5.38 (0.5342)	2.30 (0.6368)
5p	−6.87	−2.52	−3.56	−4.69	—	2.04	
5s	−10.40	−5.45	−6.69	−8.03	—	2.08	
Rh 4d	−12.50	−9.65	−11.31	−12.83	−14.12	4.29 (0.5807)	1.97 (0.5685)
5p	−4.70	−2.86	−3.84	−4.73	−5.50	1.98	
5s	−8.09	−6.04	−7.21	−8.29	−9.21	2.02	

[a] Two Slater exponents are listed for d functions. Each is followed in parentheses by its coefficient in the double-zeta expansion.

Table 3 Details of sulfur charge iterations

Complex	Orbital	H_{ii}/eV					Exponent ζ_1
		Default	+1	+2	+3	+4	
Mo	S 3p	−13.3000	−12.72	−13.17	—	—	1.82700
	3s	−20.0000	−23.28	−23.78	—	—	2.12200
Tc	S 3p	−13.3000	−12.67	−13.15	—	—	1.82700
	3s	−20.0000	−23.23	−23.71	—	—	2.12200
Ru	S 3p	−13.3000	−12.61	−13.13	−13.65	—	1.82700
	3s	−20.0000	−23.17	−23.70	−24.21	—	2.12200
Rh	S 3p	−13.3000	−12.66	−13.19	−13.76	−14.25	1.82700
	3s	−20.0000	−23.22	−23.75	−24.31	−24.81	2.12200

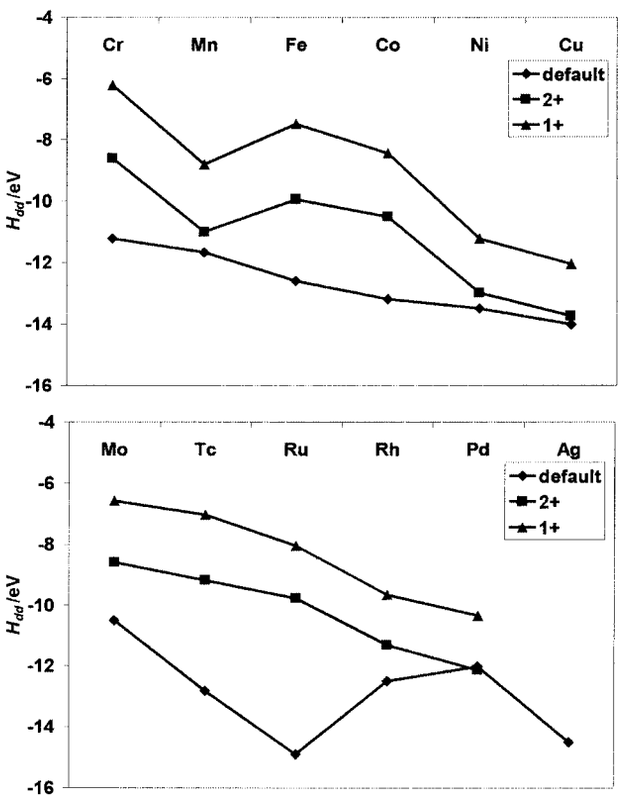

Fig. 3 Periodic trends in d-orbital energies (charge iterated and default) for first row (top) and second row (bottom) transition metal bis-9S3 complexes $[M(9S3)_2]^+$ and $[M(9S3)_2]^{2+}$.

bonding effects are likely to increase on moving from right to left in the series. Thirdly, the H_{dd} values for a given M^{2+} complex increase, by a similar amount, upon the addition of an electron to give the corresponding M^+ complex. Thus, π-backbonding effects are likely to increase upon reduction from M^{2+} to M^+. This is particularly relevant to the complexes of Tc and Re where this reduction results in C–S bond cleavage. It is less relevant later in the series as the e_g orbitals begin to be populated.

Mulliken overlap populations of C–S bonds. The charge iterated H_{ii} parameters were used for Mulliken population analysis of $[M(9S3)_2]^{2+}$ and $[M(9S3)_2]^+$ complexes of a series of second-row metals chosen to embrace the transition from unreactive C–S bonds (Rh, Ru) to reactive ones (Tc and by extrapolation, Mo). The Mulliken overlap populations of the C–S bonds can be taken to parallel the relative C–S bond strengths throughout the series; a larger overlap population indicates a stronger bond, and hence, upon relaxation of the artificial geometric constraints (Table 1), a shorter bond. Moreover, within each complex, separate Mulliken overlap populations may be computed for the "in-plane" and "out of plane" C–S bonds, and compared with the crystallographic bond lengths. The overlap populations of the C–S bonds in free 9S3 were also calculated. The results of the analysis are shown in Fig. 4. In free 9S3, constrained to the C_3 conformation found in the complexes, each sulfur atom has two non-equivalent C–S bonds, corresponding to the in-plane and out-of-plane bonds in the complexed form. These two bonds have different overlap populations, 0.662 and 0.666 respectively. The difference is the result of ring conformational effects and not C–S bond

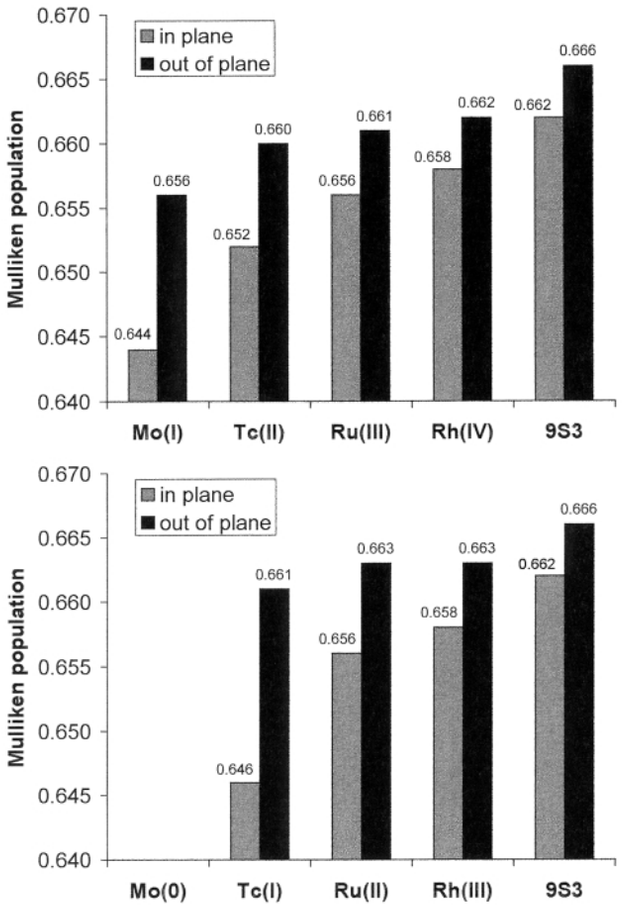

Fig. 4 Trends in C–S Mulliken overlap populations for d^5 (top) and d^6 (bottom) $[M(9S3)_2]^{n+}$ complexes, in (grey) and out (black) of plane. Values for the molybdenum(0) complex were not determined.

distances since the latter are identical between the two types of C–S bond. The populations decrease upon complexation with the metals, consistent with the experimental observation that the C–S bonds are longer in the M^{2+} complexes than in free 9S3. The population decrease (averaged over in-plane and out-of-plane C–S bonds) is more significant for the d^6 complexes than for their d^5 analogues, consistent with the expected stronger back donation by the more reduced metal centre. It is more significant for the in-plane C–S bonds than for the out-of-plane bonds, consistent with the crystallographic finding that the in-plane C–S bonds are longer than the out-of-plane bonds in the M^{2+} complexes. Finally, the reduction in the in-plane C–S overlap population increases smoothly on moving to the left from Ru through Tc to Mo (for both the d^5 and the d^6 series), as expected from the trends in d-orbital energies.

Fragment molecular orbital analysis. The complex $[Tc(9S3)_2]^{2+}$ was used for the initial FMO calculation. The approach was then repeated for other metal centres, as before using the same geometric model in each case. Three molecular fragments were defined: the metal atom (fragment 1, FMOs 1–9) and the two ligands (fragment 2, FMOs 10–57 and fragment 3, FMOs 58–105). These fragments were allowed to interact to produce a set of molecular orbitals (MOs) describing the complex as a whole (Fig. 5). Each "free" ligand fragment was found to have two degenerate orbitals (FMO no. 37 and 38 in fragment 2, and 85 and 86 in fragment 3) at −1.25 eV corresponding to the LUMO of the fragments. The C–S σ* character of these degenerate FMOs is depicted by the density plot in the plane of one in-plane C–S bond shown in Fig. 6, and three-dimensionally for the ligand as a whole in Fig. 7. Combinations of the metal d_{xy}, d_{yz} and d_{xz} orbitals of the metal fragment (FMOs 3, 4, and 5) have the correct symmetry to interact with these ligand

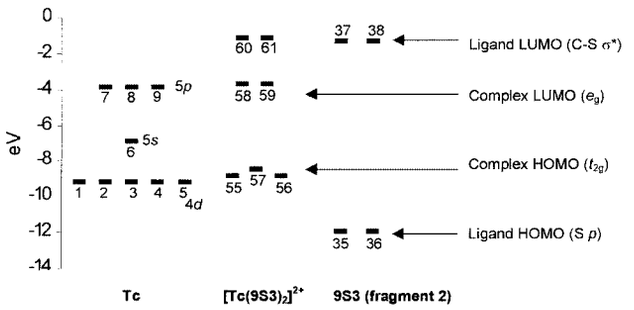

Fig. 5 Partial MO diagram for $[Tc(9S3)_2]^{2+}$ to show interaction between metal 4d-orbitals (FMOs 1–5; 3,4 and 5 have t_{2g} character) and ligand LUMO orbitals. For simplicity, ligand HOMO (FMOs 35, 36) and LUMO (FMOs 37, 38) orbitals from only one 9S3 (fragment 2) are shown.

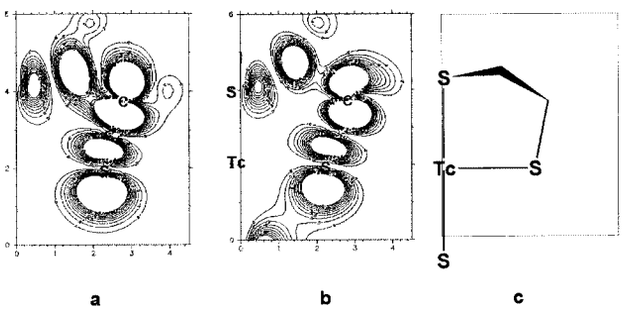

Fig. 6 Density plot for FMO 37 (the LUMO of a 9S3 ligand) showing C–S antibonding character.

fragment LUMOs. The overlap of these FMOs in the Tc^{2+} complex gives rise to a set of filled MOs of largely metal t_{2g} character (but also significant C–S σ* character, as discussed below). These comprise the HOMO of the complex (a single orbital MO57, −8.44 eV) and a degenerate pair of orbitals slightly lower in energy (MO55 and MO56, −8.78 eV). The LUMO of the complex (MO58 and MO59) corresponds to the degenerate metal 4d orbitals of e_g character (−3.67 eV) and has no significant contribution from the ligand FMOs 37, 38, 85 and 86. The next lowest molecular orbitals (MO60–61, −1.14 eV) have largely ligand C–S σ* (FMOs 37, 38, 85, 86) character.

FMO populations. Having identified the relevant ligand fragment orbitals and their interactions with the metal, it is instructive to observe the effect of metal co-ordination upon their FMO populations. In free 9S3 the population of FMOs 37, 38, 85 and 86 is zero, but in the complex they become significantly populated. Fig. 8 shows the FMO population of FMO 37 (as an example), and the overlap coefficient representing its contribution to MO55, for the second row metal d^5 and d^6 complexes. For both the d^5 and d^6 series there is a trend towards increasing the population of FMO 37 on moving to the left in the period. Similar behaviour is observed for FMOs 38, 85 and 86. Also, predictably, there is a significant increase in the FMO population of FMO 37 on moving from the d^5 to the d^6 series. This effect is a consequence of both the increase in number of t_{2g} electrons and the expansion and energy increase of the t_{2g} orbital. The latter is probably the main contributor since the 20% increase in electron number (from 5 to 6) cannot account for the large increase in population of FMO 37 (from 0.032 to 0.055, around 70%, in the case of technetium). Thus, although the calculated populations of the C–S σ* orbitals are small (probably reflecting the over-estimation of HOMO–LUMO energy differences typical of the EHT method), the calculated trends in involvement and occupancy of the ligand orbitals with C–S σ* character parallel the experimental trends[1] in C–S bond lengthening and activation. Thus, the combined computational and experimental results support the role of π-back donation in this process.

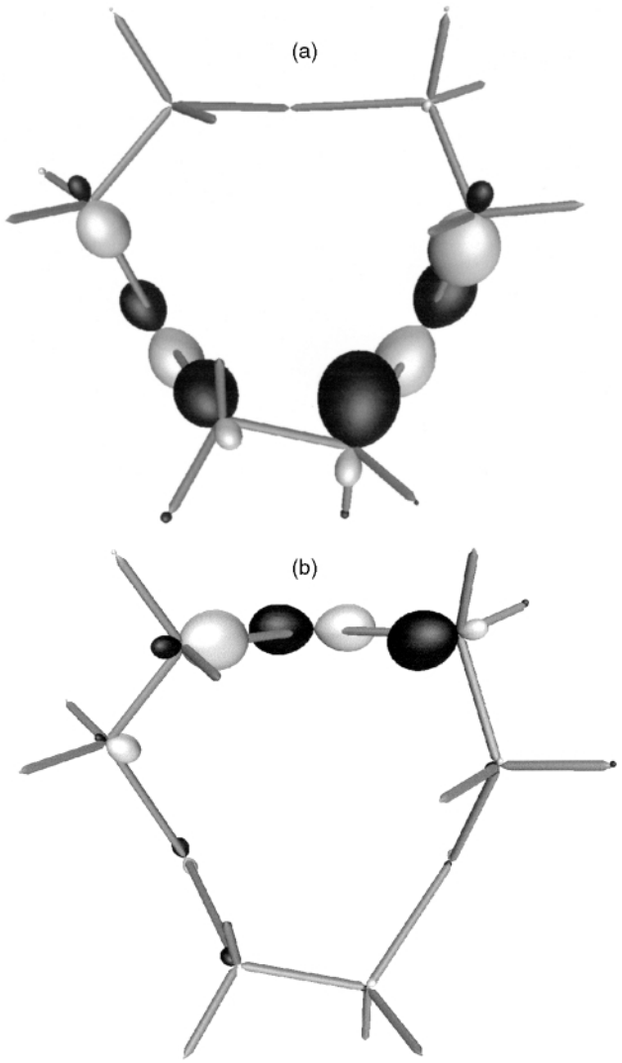

Fig. 7 Three-dimensional representation of degenerate FMOs 37 (a) and 38 (b) for one 9S3 ligand (fragment 2).

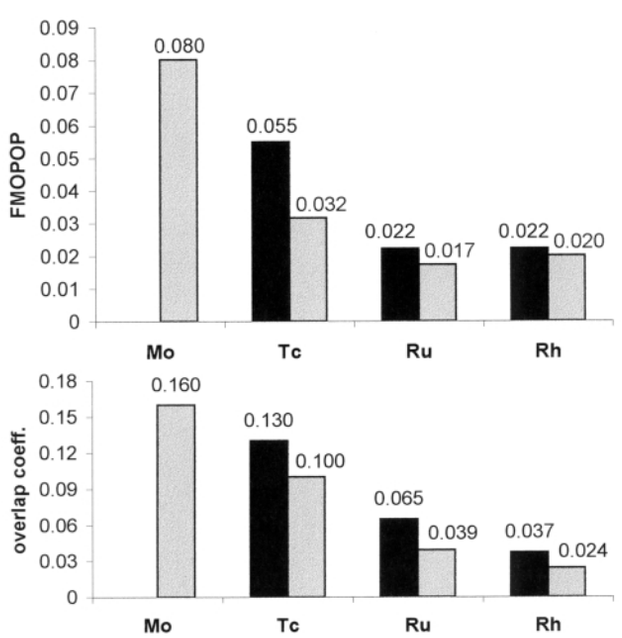

Fig. 8 Top: FMO population of FMO 37 (ligand LUMO with C–S σ* character). Bottom: coefficients of FMO 37 in MO55 (metal t_{2g} combination) for d^5 (grey) and d^6 (black) 4d transition metals. Both the populations and the coefficients increase on reduction from d^5 to d^6 and on moving to the left in the period (*i.e.* increasing d-orbital energy).

Electrospray mass spectra

The above analysis presents a model for the thermal loss of ethene from $[Re(9S3)_2]^+$ and $[Tc(9S3)_2]^+$ in which C–S bonds are weakened by π-back donation into C–S antibonding orbitals to the extent that room-temperature thermal vibration is sufficient to cleave a pair of C–S bonds. According to this model, in analogous d^6 complexes of later metals much stronger thermal vibrations would be required to overcome the stronger C–S bonds, and hence ethene loss is not observed. As a possible means of investigating this possibility of unimolecular thermal fragmentation of the ligand in the complexes, in a situation devoid of co-reactants, electrospray mass spectroscopy was employed. Applications of this technique in the field of metal complexes have been reviewed previously.[13] In ES-MS the ionisation of the sample can be made "harder" or "softer" by varying the potential applied to the skimmer cone, for example to control the degree of dissociation of carbon monoxide from metal carbonyl complexes in the mass spectrometer.[14] This method of promoting "in-source" fragmentation is thought to be through the drying gas acting also as a collision gas. Increasing the cone voltage then effectively increases the collision energy, thus increasing the degree of fragmentation in a readily controllable way.[13] In the present investigation it was therefore anticipated that the degree of fragmentation (*e.g.* ethene loss) would increase with the applied potential, and that the relative extent of ethene loss at comparable potentials would be greater towards the left of the series and for lower oxidation states, as predicted by the calculations. Spectra of $[M(9S3)_2]^{2+}$ (M = Tc, Re, Ru or Os) were recorded using the first quadrupole of the QUATTRO II "triple" quadrupole mass spectrometer to compare their fragmentation patterns at different cone voltages (10, 30, 50 and 100 V). The approach was successful in generating different degrees of fragmentation, with higher voltages giving more fragmentation on these samples. At moderate cone voltages the fragmentation observed was almost all attributable to loss of one or more ethene moieties. Representative spectra of complexes of Ru and Tc are shown in Figs. 9 and 10 respectively; the complexes of Re and Os exhibited qualitatively similar behaviour and are not shown.

Ruthenium. The ruthenium complex gave no fragmentation at 10 V: the major species observed were $[Ru(9S3)_2{\cdot}PF_6]^+$ (m/z = 606.9, calc. 606.9), $[Ru(9S3)_2{\cdot}MeCN]^{2+}$ (m/z = 251.2, calc. 251.5) and $[Ru(9S3)_2]^{2+}$ (m/z = 230.6, calc. 231.0). At 30 V small additional peaks were observed due to loss of ethene to give ions containing the $[Ru(9S3)L]^{2+}$ (L = $SCH_2CH_2SCH_2$-CH_2S) core: $[Ru(9S3)L{\cdot}MeCN]^{2+}$ (m/z = 237.2, calc. 237.5) and $[Ru(9S3)L]^{2+}$ (m/z = 216.6, calc. 216.9). At 50 V ethene loss was extensive and at 100 V the spectra became much more complex and were not interpreted.

Technetium. The technetium complex showed a more complex pattern even at 10 V: as well as ions corresponding to $[Tc(9S3)_2{\cdot}BF_4]^+$ (m/z = 545.9), $[Tc(9S3)_2{\cdot}MeCN]^{2+}$ (m/z = 250.0) and $[Tc(9S3)_2]^{2+}$ (m/z = 229.5), a significant peak corresponding to $[Tc(9S3)L]^+$ (m/z = 430.8) and a very small peak corresponding to $[Tc(9S3)_2]^+$ (m/z = 458.8) were observed. This could be accounted for by the hypothesis that during the ionisation process $[Tc(9S3)_2]^{2+}$ acquires an electron (perhaps from Fe^{2+} ions entering the solution by electrolysis in the steel capillary[15]) to produce $[Tc(9S3)_2]^+$, almost all of which loses ethene to produce $[Tc(9S3)L]^+$. This observation would be consistent with the solution chemistry and the calculations, in that the d^6 technetium complex loses ethene much more readily than the d^5 technetium species. At 30 V, fragmentation of $[Tc(9S3)_2]^{2+}$ is much more extensive than that of the ruthenium analogue at the same voltage: fragments corresponding to $[Tc(9S3)L]^{2+}$ (m/z = 215.4) and $[Tc(9S3)L{\cdot}MeCN]^{2+}$ (m/z = 235.9) each have a relative abundance greater than 70% in the

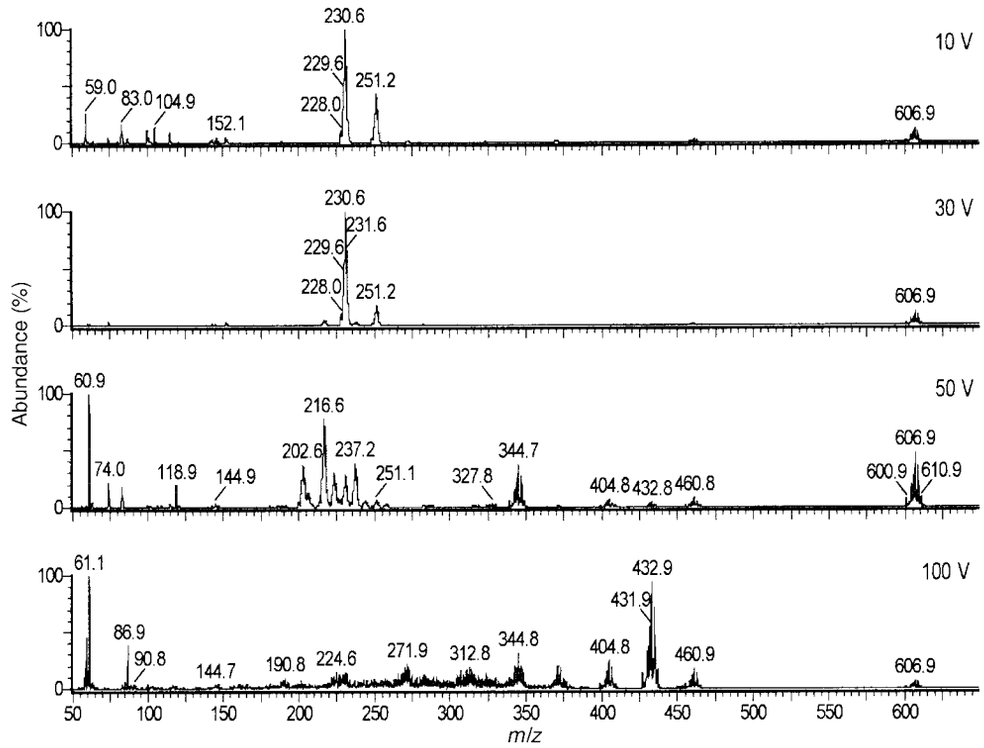

Fig. 9 Electrospray mass spectra of $[Ru(9S3)_2][PF_6]_2$ at various cone voltages (10 to 100 V).

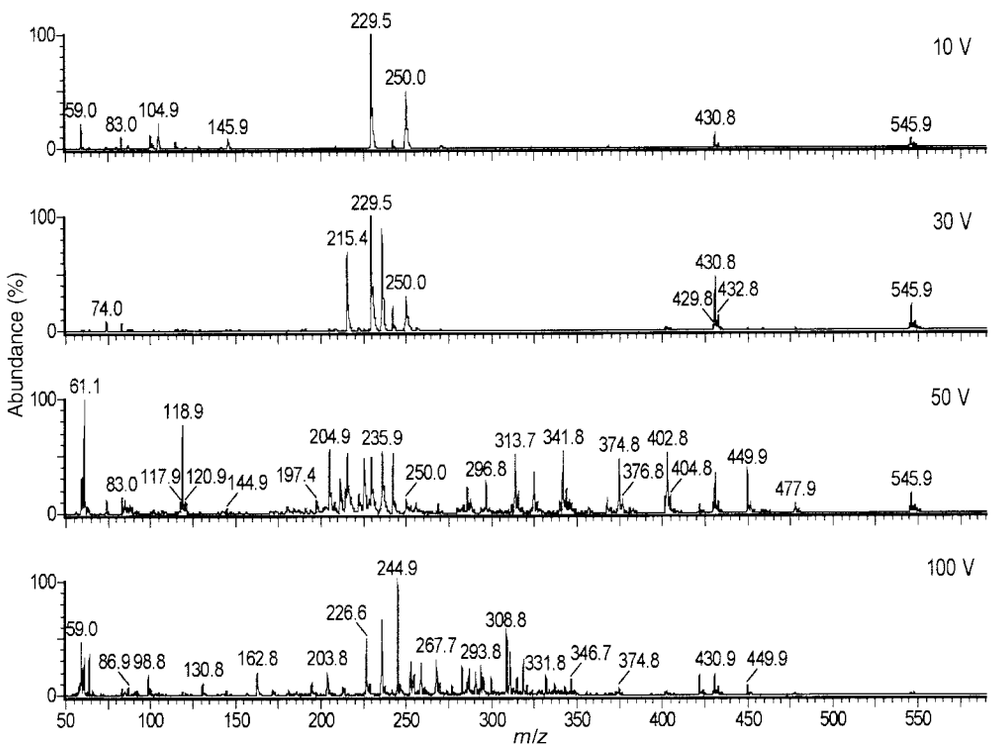

Fig. 10 Electrospray mass spectra of $[Tc(9S3)_2][BF_4]_2$ at various cone voltages (10 to 100 V).

spectrum. Once again, at still higher voltages the fragmentation is more extensive and the spectra are complex.

A comparative summary of the tendency to lose ethene among these complexes at 10 and 30 V is shown in Fig. 11. This diagram expresses the % of the detected ions made up of intact and fragmented (*i.e.* having lost one or more ethene units) complex ions. For example, the % of intact $[Tc(9S3)_2]^{2+}$ complex is calculated from the relative abundances according to expression (2). Fig. 11 shows a trend that is consistent with both the EHT calculations (which predict that $[Tc(9S3)_2]^{2+}$ fragments more readily than $[Ru(9S3)_2]^{2+}$) and with established group trends (which imply that third row metals are better back donors than second row metals, thus $[Tc(9S3)_2]^{2+}$ fragments less readily than $[Re(9S3)_2]^{2+}$, and likewise for Ru and Os).

$$\frac{[Tc(9S3)_2]^{2+} + [Tc(9S3)_2(BF_4)]^{+} + [Tc(9S3)_2{\cdot}MeCN]^{2+}}{\sum_{n=0,1,2\ldots} [Tc(9S3)_2 - n(C_2H_4)]^{2+} + [Tc(9S3)_2(BF_4) - n(C_2H_4)]^{+} + [Tc(9S3)_2{\cdot}MeCN - n(C_2H_4)]^{2+}} \times 100\% \quad (2)$$

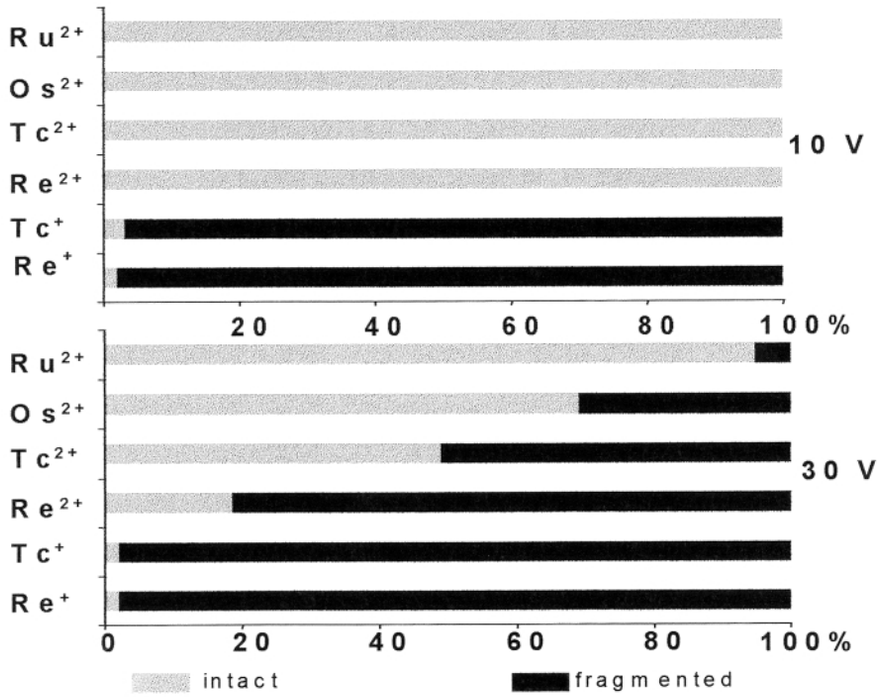

Fig. 11 Total relative abundance of ions containing the intact $[M(9S3)_2]^{n+}$ core and ethene loss product ions (see text for full explanation) in the electrospray mass spectra (Quattro instrument) at 10 and 30 V cone voltages. The abundance of the intact $[Tc(9S3)_2]^+$ and $[Re(9S3)_2]^+$ ions (both less than 1%) has been exaggerated for the purposes of this diagram.

Results and trends similar to those shown in Fig. 11 were also observed using the Finnigan MAT LCQ electrospray mass spectrometer. On this instrument different needle voltages were applied (15, 50, 75 and 100 V). Unlike experiments performed on the Quattro II, where the samples were dissolved and injected into a mobile phase of dry acetonitrile, the samples in the Finnigan MAT LCQ experiments were dissolved in acetonitrile and injected into a mobile phase of methanol–water (1:1). Consequently no ions corresponding to the acetonitrile adducts observed on the Quattro II instrument were seen. Nevertheless, these trends are consistent with the trends observed in the extended Hückel calculations.

Tandem mass spectrometry (ES-TMS) was also performed on the Quattro II instrument to confirm that the apparent loss of 28 Daltons (or 14 apparent mass units when the ion is doubly charged) is a direct result of fragmentation of $[M(9S3)_2]^{2+}$ ions formed in the initial electrospray ionisation, by loss of ethene units. These experiments confirmed the losses of 28 from the $[M(9S3)_2]^{2+}$ ions (M = Tc, Ru, Re or Os), but, so far, not sequential formation of $[Tc(9S3)_2]^+$ and $[Tc(9S3)L]^+$ from $[Tc(9S3)_2]^{2+}$ because of insufficient sensitivity. At 0 eV collision energy the parent ions $[M(9S3)_2]^{2+}$ pass through the collision cell without fragmentation. On increasing the collision energy to 10 eV a mild fragmentation (ethene loss) is observed for $[M(9S3)_2]^{2+}$ (M = Ru, Tc or Os), though the parent ion is the most abundant while ions corresponding to the loss of one ethene unit are of low intensity. However $[Re(9S3)_2]^{2+}$, at a collision energy of only 10 eV, already shows $[Re(9S3)L]^{2+}$ (loss of one ethene molecule) as the base peak. A small peak corresponding to the loss of a second ethene unit is also observed. When the collision energy is increased to 20 eV the fragmentation patterns for $[M(9S3)_2]^{2+}$ (M = Ru, Tc or Os) are again similar only now the base peak corresponds to $[M(9S3)L]^+$ ion (loss of one ethene). At the same potential (20 V), $[Re(9S3)_2]^{2+}$ exhibits much more extensive fragmentation, with an ion corresponding to the loss of three ethene molecules as the base peak.

In conclusion, extended Hückel calculations predict that carbon–sulfur bonds in transition metal complexes $[M(9S3)_2]^{n+}$ are weaker than in free 9S3, and that the technetium(I) and rhenium(I) complexes possess the weakest C–S bonds, followed by the technetium(II) and rhenium(II) complexes, while the C–S bonds in d^5 and d^6 complexes of later transition metals are weakened much less significantly. These predictions are confirmed by the solution chemistry, crystallographic data, and electrospray mass spectrometry. These theoretical and experimental studies together provide strong support for the hypothesis that π-back donation by the metal into ligand orbitals with C–S antibonding character causes lengthening and activation of ligand C–S bonds. The mild and highly controllable nature of the electrospray mass spectrometry ionisation process provides a valuable tool for the investigation of activation energy trends for intramolecular dissociation processes in series of analogous complexes.

Experimental

Synthesis of complexes

All syntheses were carried out under dry dinitrogen, using dried and degassed solvents, but subsequent manipulations and separations were carried out in air. The compounds $RuCl_3 \cdot 3H_2O$, $Na_2[OsCl_6]$, $Fe[ClO_4]_3 \cdot 6H_2O$, $Na[PF_6]$, $[NH_4][PF_6]$, ethanol (absolute), methanol (anhydrous), dimethyl sulfoxide (AR) and acetonitrile (anhydrous) were purchased from Aldrich while 2-methyl-5-(1-methylethyl)cyclohexa-1,3-diene (*α*-phellandrene) was from Fluka. The preparation of $[Re(9S3)_2][BF_4]_2$[16] and $[Tc(9S3)_2][BF_4]_2$[17] has been described previously. Treatment of $[Re(9S3)_2][BF_4]_2$ with $[NH_4][PF_6]$ in MeCN results in counter-ion metathesis to afford $[Re(9S3)_2][PF_6]_2$; $[Ru(9S3)_2][PF_6]_2$ was prepared as previously described.[18] The osmium complex $[Os(9S3)_2][PF_6]_2$ was prepared from $[Os_2Cl_4(p\text{-}MeC_6H_4CHMe_2)_2]$,[19] as previously described.[20]

Electrospray mass spectroscopy

Electrospray and tandem mass spectrometry measurements were carried out at the EPSRC National Mass Spectrometry Service Centre (Chemistry Department, University of Wales, Swansea) on a QUATTRO II "triple" quadrupole (Micromass, Cheshire, UK). Samples ($[M(9S3)_2][X]_2$, M = Tc, Ru, Re or Os, X = BF_4 or PF_6) in anhydrous acetonitrile solution were loop-injected into a stream of dry acetonitrile and

transferred into the mass spectrometer at a flow rate 0.02 cm^3 min^{-1} *via* a steel capillary which was heated to 60 °C and a voltage of +3.5 kV was applied. Nitrogen was used as the sheath gas to assist nebulisation and also as drying gas to promote solvent evaporation. Two types of experiment were performed with this instrument: electrospray mass spectrometry and electrospray tandem mass spectrometry. In the ES-MS experiment different degrees of in-source fragmentation were induced by varying the cone voltage between 10 and 100 V. A sample was injected and the spectra recorded for the different cone voltages (10, 30, 50 and 100 V) consecutively on the same sample. The fragmentation patterns of the complexes at the different cone voltages were then compared. In the ES-TMS experiment the cone voltage was fixed at 15 V to minimise in-source fragmentation of the complexes and optimise the parent ion. The ions corresponding to $[M(9S3)_2]^{2+}$ were selected by the first quadrupole and then passed through the collision cell at varying collision-induced dissociation (CID) energies (typically between 10 and 30 eV). Argon was used as the collision gas, with a cell pressure of 10^{-3} mbar. The daughter ions obtained at different CID energies were compared.

Electrospray mass spectra were also recorded on a Finnigan MAT LCQ ion trap mass spectrometer (University of Kent Department of Biosciences, Wellcome Trust Protein Science Facility). Samples of the same complexes were dissolved in MeCN and injected, *via* a Valco valve fitted with a 10 μl loop, into a water–methanol mobile phase at a flow rate of 0.02 cm^3 min^{-1}. The nebuliser tip was at a voltage of +3.5 kV, with nitrogen used both as a drying and nebulising gas. The capillary was heated to 60 °C and the voltage was varied between 10 and 100 V for all the complexes to induce different degrees of fragmentation. Fresh samples were injected every time the needle voltage was altered. The fragmentation patterns of the complexes at different needle voltages were compared.

EHT-MO calculations

All calculations were performed on an Indigo^2 R10000 Silicon Graphics workstation using the extended Hückel (EH) program MEHMACC.[21] The program performs self-consistent charge iterations to adjust orbital energies H_{ii} based on Valence Orbital Ionisation Potentials (VOIP).[22–24] Charge iterations were performed for valence orbital energies of the transition metals (d, s, p) and sulfur (s, p), while standard parameters were used for valence orbitals of carbon (2s: $H_{ii} = -21.4000$ eV, $\zeta_1 = 1.62500$, $c_1 = 1.00000$; 2p: $H_{ii} = -11.4000$ eV, $\zeta_1 = 1.62500$, $c_1 = 1.00000$) and hydrogen atoms (1s: $H_{ii} = -13.6000$, $\zeta_1 = 1.30000$, $c_1 = 1.00000$). The program was used to calculate molecular orbitals, Mulliken populations,[25] fragment molecular orbitals, fragment molecular orbital populations, and for the representation of density plots. Visualisation of the molecular orbitals corresponding to the C–S σ* orbitals was obtained by plotting the respective 3-dimensional matrix grid † using the graphics package Geomview.[26]

An idealised model structure was defined using average ligand bond lengths from the $[Ru(9S3)_2]^{2+}$ structure[27] (shown in Table 1 and Fig. 2) and bond angles and torsional angles taken from an average over all first and second row structures.[10] The model C–S bond distances are within 0.013 Å of all the crystallographically determined distances.[10]

Acknowledgements

We thank the EPSRC for a studentship and for a fieldwork grant (to G. E. D. M.).

† Program reads the coefficients of a selected molecular orbital from a MEHMACC output file and calculates a graphical matrix grid that can be read by the package Geomview.

References

1 G. E. D. Mullen, M. J. Went, S. Wocadlo, A. K. Powell and P. J. Blower, *Angew. Chem., Int. Ed. Engl.*, 1997, **36**, 1205.
2 S. K. Ibrahim and C. J. Pickett, *J. Chem. Soc., Chem. Commun.*, 1991, 246; D. Sellmann and W. Reisser, *J. Organomet. Chem.*, 1985, **297**, 319; M. Cha, S. C. Shoner and J. A. Kovacs, *Inorg. Chem.*, 1993, **32**, 1860; J. T. Goodman and T. B. Rauchfuss, *J. Am. Chem. Soc.*, 1999, **121**, 5017.
3 D. L. Dubois, W. K. Miller and M. Rakowski-Dubois, *J. Am. Chem. Soc.*, 1981, **103**, 3429; P. J. Blower, J. R. Dilworth, J. P. Hutchinson, T. Nicholson and J. A. Zubieta, *J. Chem. Soc., Dalton Trans.*, 1986, 1339.
4 R. D. Adams, L. Chen and J. H. Yamamoto, *Organometallics*, 1995, **14**, 3704; R. D. Adams, S. B. Falloon and K. McBride, *Organometallics*, 1995, **14**, 1739; S. Rossi, K. Kalinen. J. Pursianen, T. T. Pakkanen and T. A. Pakkanen, *J. Organomet. Chem.*, 1992, **440**, 367; R. D. Adams, L. Chen and J. H. Yamamoto, *Inorg. Chim. Acta*, 1995, **229**, 47; D. Sellmann, F. Knoch and C. Wronna, *Angew. Chem., Int. Ed. Engl.*, 1988, **27**, 689.
5 A. J. Blake, A. J. Holder, T. I. Hyde, H.-J. Küppers, M. Schröder, S. Stötzel and K. Wieghardt, *J. Chem. Soc., Chem. Commun.*, 1989, 1600; M. A. Bennett, L. Y. Goh and A. C. Willis, *J. Chem. Soc., Chem. Commun.*, 1979, 32; *J. Am. Chem. Soc.*, 1996, **118**, 4984.
6 D. S. Marynick, *J. Am. Chem. Soc.*, 1984, **106**, 4064; S.-X. Xiao, W. C. Trogler, D. E. Ellis and Z. Berkovitch-Yellin, *J. Am. Chem. Soc.*, 1983, **105**, 7033.
7 A. G. Orpen and N. G. Connelly, *J. Chem. Soc., Chem. Commun.*, 1985, 1310.
8 S. R. Cooper and S. C. Rawle, *Struct. Bonding* (*Berlin*), 1990, **72**, 1; A. J. Blake and M. Schröder, *Adv. Inorg. Chem.*, 1990, **35**, 1.
9 H.-B. Kraatz, H. Jacobsen, T. Ziegler and P. H. Boorman, *Organometallics*, 1993, **12**, 76; J. Giner Planas, M. Hirano and S. Komiya, *Chem. Commun.*, 1999, 1793; S. Harris and R. R. Chianelli, *J. Catal.*, 1984, **86**, 400; L. Dong, S. B. Duckett, K. F. Ohman and W. D. Jones, *J. Am. Chem. Soc.*, 1992, **114**, 151.
10 Data obtained from The Director, Cambridge Crystallographic Data Centre, 12 Union Rd, Cambridge CB2 1EZ, UK (fax: +44 (0) 1223 336 033; e-mail: deposit@chemcrys.cam.ac.uk).
11 For relevant reviews see: H. C. Friedmann, A. Klein and R. K. Thauer, *FEMS Microbiol. Rev.*, 1990, **87**, 339; H. Tops, B. S. Clausen and F. E. Massoth, *Hydrotreating Catalysis*, *Science and Technology*, Springer, Berlin, 1996; D. D. Whitehurst, T. Isoda and I. Mochida, *Adv. Catal.*, 1998, **42**, 345; K. Tatsumi and H. Kawaguchi, *ACS Symp. Ser.*, 1996, **653**, 310.
12 R. Hoffmann, J. M. Howell and E. L. Muetterties, *J. Am. Chem. Soc.*, 1972, **94**, 3047.
13 W. Henderson, B. K. Nicholson and L. J. McCaffrey, *Polyhedron*, 1998, **17**, 4291.
14 W. Henderson, J. S. McIndoe, B. K. Nicholson and P. J. Dyson, *J. Chem. Soc., Dalton Trans.*, 1998, 519.
15 M. G. Ikonomou, A. T. Blades and P. Kebarle, *Anal. Chem.*, 1991, **63**, 1989.
16 S. O. C. Matondo, P. Mountford, D. J. Watkin, W. B. Jones and S. R. Cooper, *J. Chem. Soc., Chem. Commun.*, 1995, 161.
17 D. J. White, H.-J. Küppers, A. J. Edwards, D. J. Watkin and S. R. Cooper, *Inorg. Chem.*, 1992, **31**, 5351.
18 M. N. Bell, A. J. Blake, M. Schröder, H.-J. Küppers and K. Wieghardt, *Angew. Chem., Int. Ed. Engl.*, 1987, **26**, 250.
19 J. A. Cabeza and P. M. Maitlis, *J. Chem. Soc., Dalton Trans.*, 1985, 573.
20 M. N. Bell, A. J. Blake, R. M. Christie, R. O. Gould, A. J. Holder, T. I. Hyde, M. Schröder and L. J. Yellowlees, *J. Chem. Soc., Dalton Trans.*, 1992, 2977.
21 Program MEHMACC, U. Häussermann, S. Wengert, R. Nesper and T. F. Fässler, ETH, Zürich, 1993; MEHMACC is based on the extended-Hückel program EHMACC, M.-H. Whangbo, M. Evain, T. Hughbanks, M. Kertes, S. Wijeyesekera, C. Wilker, C. Zheng and R. Hoffmann, 1990 and is available under mehmacc@inorg.chem.ethz.ch.
22 H. Basche, A. Viste and H. B. Gray, *J. Chem. Phys.*, 1966, **44**, 10.
23 U. Häussermann, PhD Thesis, ETH, Zürich, 1995.
24 S. Wengert, PhD Thesis, ETH, Zürich, 1997.
25 R. S. Mulliken, *J. Chem. Phys.*, 1955, **23**, 1833.
26 Geomview 1.6.1, The Geometry Center, University of Minnesota (http://www.geom.umn.edu). M. Phillips, S. Levy and T. Munzner, *Notices of the American Methematical Society* (*Computers and Mathematics Column*), 1993, **40**, 985.
27 S. C. Rawle and S. R. Cooper, *J. Chem. Soc., Chem. Commun.*, 1987, 308.

Paper 9/05976H